


Elastic colloidal monopoles and reconfigurable self-assembly in liquid crystals

Ye Yuan¹, Qingkun Liu¹, Bohdan Senyuk¹ & Ivan I. Smalyukh^{1,2,3,4*}

Monopole-like electrostatic interactions are ubiquitous in biology¹ and condensed matter²⁻⁴, but they are often screened by counter-ions and cannot be switched from attractive to repulsive. In colloidal science, where the main goal is to develop colloidal particles^{2,3} that mimic and exceed the diversity and length scales of atomic and molecular assembly, electrostatically charged particles cannot change the sign of their surface charge or transform from monopoles to higher-order multipoles⁴. In liquid-crystal colloids⁵⁻⁷, elastic interactions between particles arise to minimize the free energy associated with elastic distortions in the long-range alignment of rod-like molecules around the particles⁵. In dipolar^{6,8}, quadrupolar⁸⁻¹² and hexadecapolar¹³ nematic colloids, the symmetries of such elastic distortions mimic both electrostatic multipoles¹⁴ and the outermost occupied electron shells of atoms^{7,15,16}. Electric and magnetic switching^{17,18}, spontaneous transformations¹⁹ and optical control²⁰ of elastic multipoles, as well as their interactions with topological defects and surface boundary conditions, have been demonstrated in such colloids²¹⁻²³. However, it has long been understood^{5,24} that elastic monopoles should relax to uniform or higher-order multipole states because of the elastic torques that they induce^{5,7}. Here we develop nematic colloids with strong elastic monopole moments and with elastic torques balanced by the optical torques induced by ambient light. We demonstrate the monopole-to-quadrupole reconfiguration of these colloidal particles by unstructured light, which resembles the driving of atoms between the ground state and various excited states. We show that the sign of the elastic monopoles can be switched, and that like-charged monopoles attract whereas oppositely charged ones repel, unlike in electrostatics¹⁴. We also demonstrate the out-of-equilibrium dynamic assembly of these colloidal particles. This diverse and surprising behaviour is explained using a model that considers the balance of the optical and elastic torques that are responsible for the excited-state elastic monopoles and may lead to light-powered active-matter systems and self-assembled nanomachines.

the axis of platelet rotation that distorts $\mathbf{n}(\mathbf{r})$. Without the influence of the confining plates, the interactions between platelets and other anisotropic colloidal objects should depend on their relative orientations, in a manner that has more structure than a simple scalar elastic charge. It will be of interest to extend and generalize our study to LC colloids without such confinement (which also causes screening of elastic interactions at large inter-particle distances) and with different geometric shapes, because the combination of LCs and particle anisotropy may lead to a richer behaviour than that observed in the electrostatic analogues of our colloids.

To conclude, we have designed, demonstrated and explained elastic colloidal monopoles in LCs, which can be induced by ambient light and have switchable sign and amplitude of the monopole moment. We have shown how like-charged elastic monopoles attract and oppositely charged ones repel, how these interactions can be switched from attractive to repulsive and how monopoles can be transformed to quadrupoles by invoking the highly reconfigurable nature of our



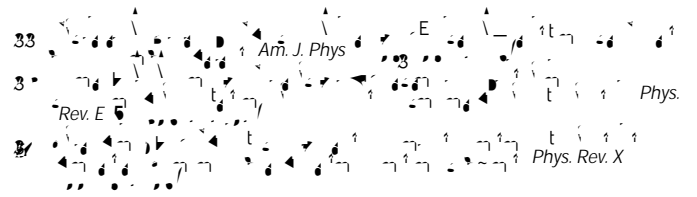
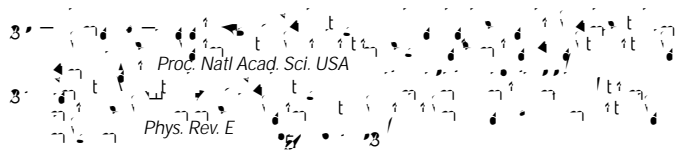
Sample preparation. The photo-responsive azobenzene molecules were synthe-

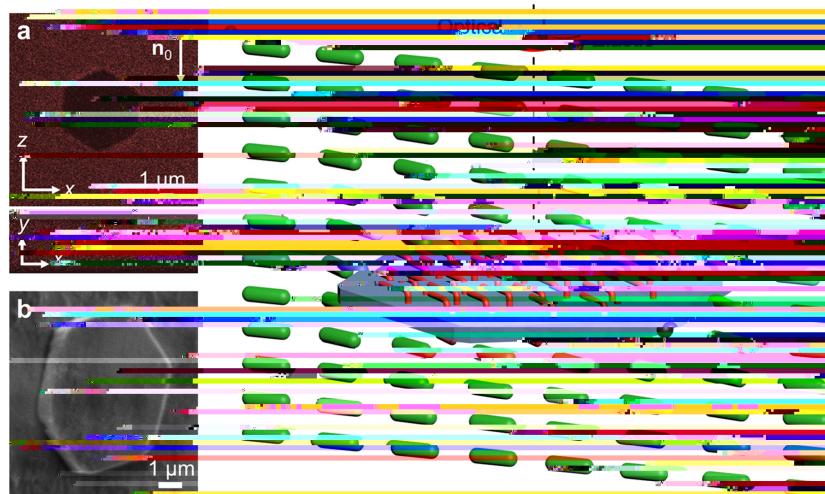
$$C_1 = \frac{2}{N} \sum_{n=1}^8 I_n \quad (7)$$

$$C = \frac{4}{N} I$$

Code availability

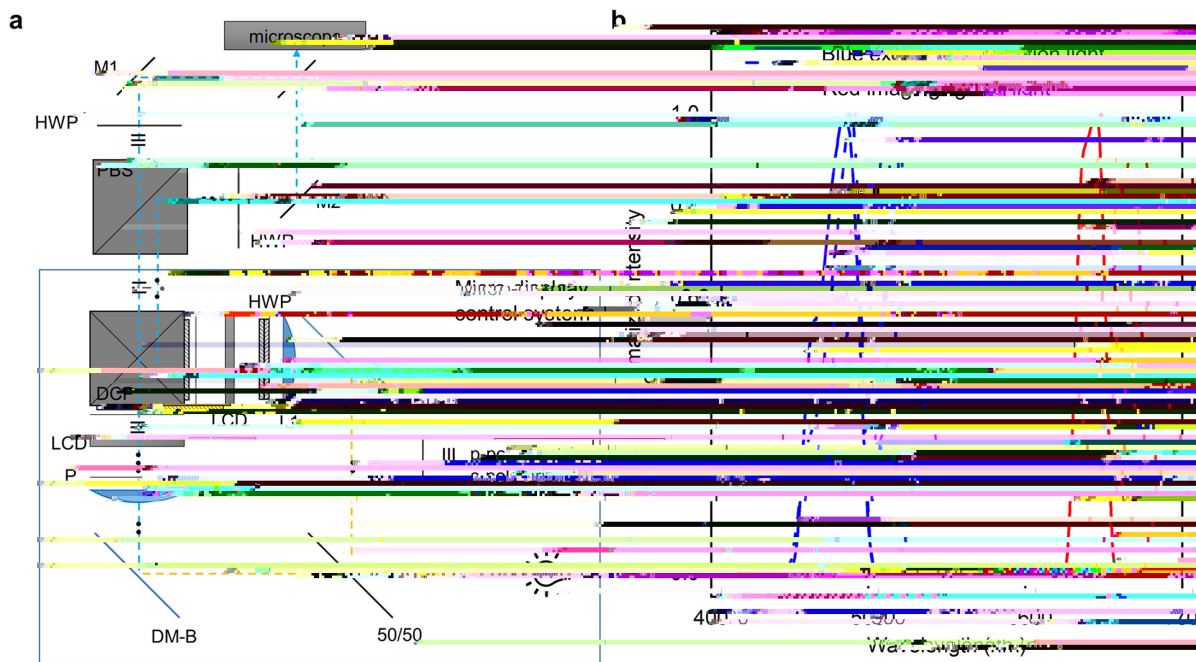
The codes used in this study for the numerical simulation and calculation are available upon request.





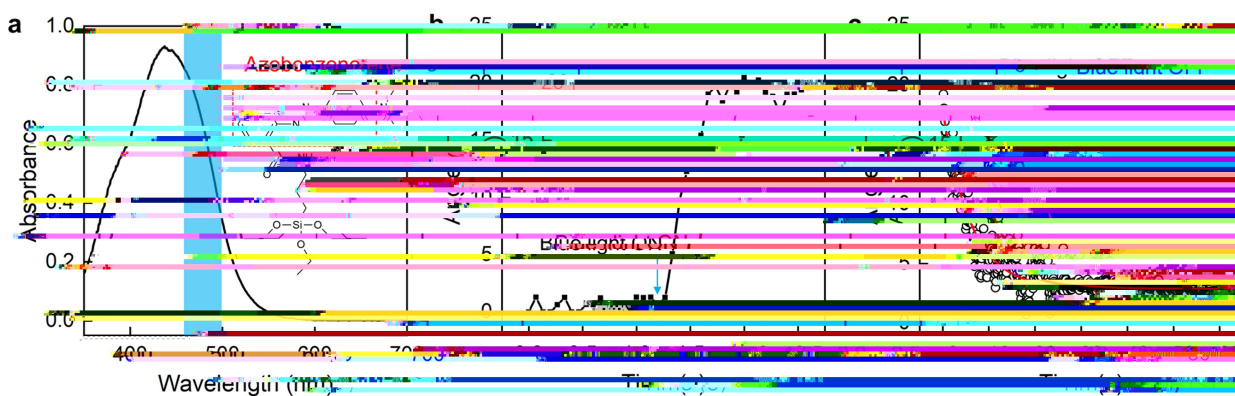
Extended Data Fig. 1 | Hexagonal colloidal platelet with azobenzene monolayers dispersed in a nematic LC. a. Three-photon excitation fluorescence microscopy images of a platelet in an LC cell, obtained at the cross-sectional plane (x - z plane) passing through the middle of the platelet, and at the vertical plane (x - y plane) that is orthogonal to the plane of the cell and the large-area faces of the platelet. Both planes pass through the centre of mass of the particle. **b.** Scanning electron microscopy image of an individual platelet placed on a substrate. **c.** Schematic of a platelet

suspended in a nematic LC. Green rods indicate the director field $\mathbf{n}(\mathbf{r})$; red rods indicate the orientation of the azobenzene molecules on the surface of the platelet; the black semi-sphere on one of the vertices of the hexagon represents the surface point defects called 'boojums'. The optical torque that rotates the platelet away from its equilibrium state is balanced by the counteracting elastic torque caused by director twisting, as shown by the blue and red curved arrows.



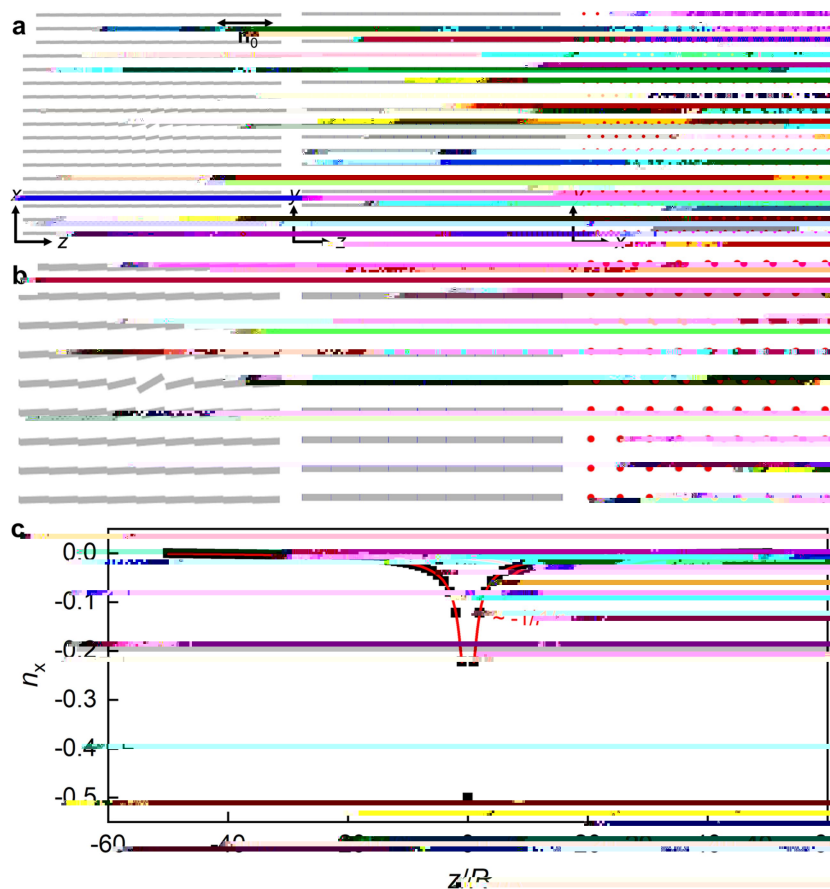
Extended Data Fig. 2 | Microdisplay-based illumination control system setup. **a.** Schematic of the optical illumination setup. White light from the lamp is split in half and directed into two optical paths using a beam splitter, filtered by two separate dichroic mirrors to supply blue light to two of the LC microdisplays (LCDs). After passing through the microdisplays, which define the spatial patterns of illumination, the two light beams are recombined by a dichroic prism and then separated again on the basis of their polarization. The two separated light paths correspond to patterns generated on the two LCDs and their polarization is further controlled by the half-wave plates. Additional mirrors enable fine-tuning of the position

of the projected patterns after the light is re-combined and coupled into the microscope. In the schematic, '50/50' denotes the plate beam splitters (BSW10R, Thorlabs); 'DM-B' indicates the dichroic mirrors that reflect blue light; L1 and L2 are convex lenses; 'HWP' denotes half-wave plates; 'P' represents the polarizer; 'DCP' is a dichroic cross-prism; 'PBS' is a cube polarizing beam splitter (CCM1-PB251, Thorlabs); M1 and M2 are silver mirrors. **b.** Spectra of the red imaging light obtained by filtering the light of the microscope lamp, and of the blue excitation light from the microdisplay control system. Solid and dashed blue lines are the spectra of the two blue channels when turned on separately.



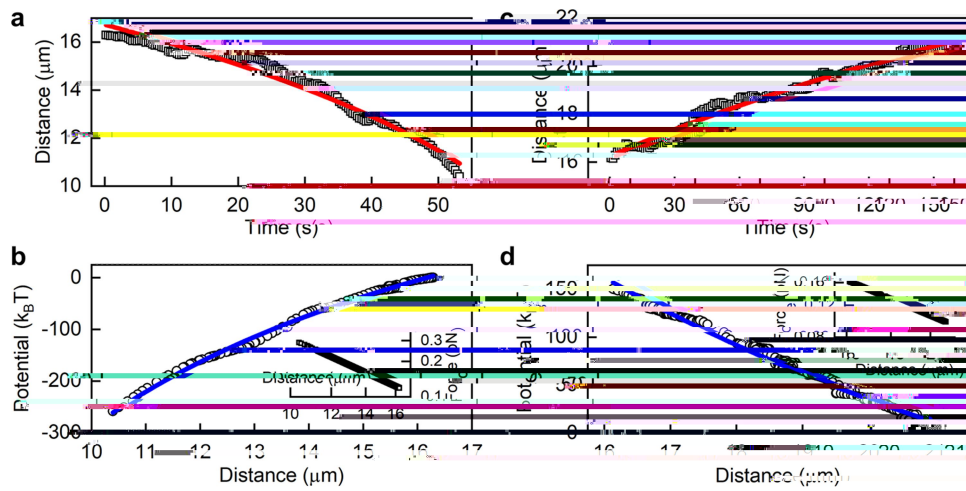
Extended Data Fig. 3 | Optical response of azobenzene-containing molecules and monopole-like platelets in a nematic LC. **a**, Absorbance spectrum of the photosensitive molecules of derivative methyl red in toluene at a concentration of 5×10^{-5} M. The spectrum was obtained using a 1-cm-thick cuvette with a spectrometer (Cary 500, Varian).

b, Time dependence of the azimuthal orientation angle of the platelet upon switching on the blue excitation light at time $t = 1.2$ s, showing how the monopole moment is turned on upon light exposure. **c**, Time dependence of the azimuthal orientation angle of the platelet relative to its equilibrium position upon switching off the blue excitation light at $t = 0$ s.



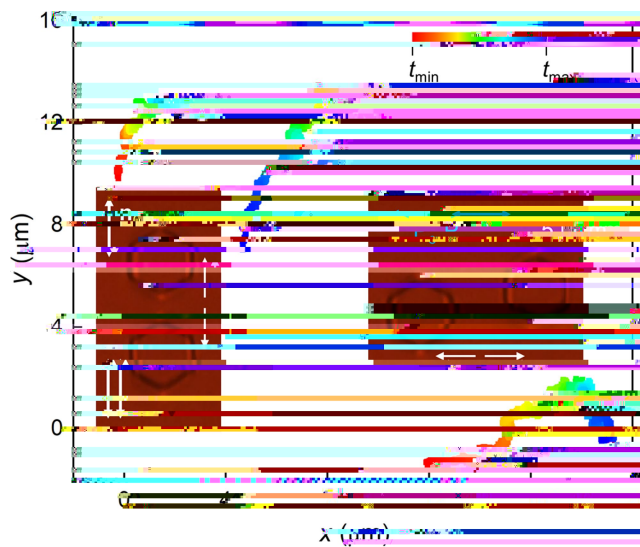
Extended Data Fig. 4 | Computer simulated director configuration of an elastic monopole. **a**, Cross-sections of the director structure in the x - z , y - z and x - y planes passing through the centre of the structure. The local director orientation is shown by grey cylinders with blue and red ends.

b, Zoomed-in view of the cross-sections shown in **a**. **c**, Distance dependence of the director deviation n_x along the z axis. The simulated results (black squares) are fitted with the function $n_x \sim -1/r$ anticipated

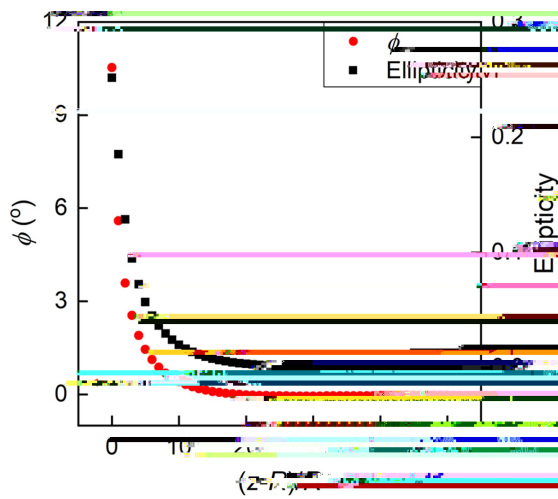


Extended Data Fig. 5 | Characterization of interactions between elastic monopoles. The strength of the elastic monopoles considered here differs from that in the main-text figures. **a, c,** Separation distance versus time of monopolar attraction (**a**) and repulsion (**c**). Red lines in **a** and **c** are the best fits of the experimental data with the function

$$r_c(t) = (r_0^3 - 3t)^{1/3} \text{ and } \text{with fitting coefficients } r_0 = 1.0709990002, \text{ and } 0.83000002, 72.78639984, 495.1796875, T_m = 3.1, T_f = 0, T_c = 0, T_d = 0.356, \text{ and } T_d = 0.356$$



Extended Data Fig. 6 | Angular dependence of quadrupolar interactions. Trajectories are colour-coded with the time elapsed since the release of the platelets from the laser traps, and the duration of interaction is $t_{\max} - t_{\min} = 100$ s. The insets are micrographs of platelets repelling each other when the separation vector that points from the centre of one particle to that of the other is roughly parallel or perpendicular to \mathbf{n}_0 . The images were taken using parallel polarizers shown by the white double arrows. By contrast, the platelets attract when the separation vector is at an angle with respect to \mathbf{n}_0 , as shown by the trajectory in the middle; the corresponding distance-versus-time dependence is shown in Fig. 4e.



Extended Data Fig. 7 | Computer-simulated polarization states of the red imaging light after passing through the sample. The angle ϕ between the long axis of the polarization ellipse and m_0 and the corresponding ellipticity are shown with red dots and black squares, respectively. The